JOURNAL OF PROPULSION AND POWER
Vol. 27, No. 2, March–April 2011

Model of High-Pressure Ablative Capillary Discharge for Plasma Thrusters

L. Pekker* and O. Pekker†
ERC Inc., Edwards Air Force Base, California 93524

DOI: 10.2514/1.49393

A zero-dimensional time-dependent high-pressure slab capillary discharge model with capillary wall thermal conduction and radiation absorption is presented. The model includes a resistor-inductor-capacitor circuit and a heat transfer radiation model based on a radiation database constructed using a commercially available radiation software, to calculate the radiation heat flux output from a uniform plasma slab. The model also includes a model of the thin transition boundary layer between the uniform plasma core and the ablative capillary walls. This transition boundary-layer model is used to obtain the boundary conditions connecting the plasma core parameters with the parameters at the ablative surface to calculate the thermal and radiation heat fluxes at the capillary walls. The radiation wall absorption coefficient is assumed to be a constant independent of wavelength and wall temperature and is an input parameter of the model. The wall thermal conductivity is also assumed to be a constant independent of the wall temperature. Thus, the model self-consistently calculates plasma parameters of the capillary discharge and distribution of wall temperature vs time. The model is used to model high-pressure ablative capillary discharge for plasma thrusters.

Nomenclature

A	=	average mass of heavy particles (neutrals and ions), au
A_a	=	mass of a neutral atom, au
A_i	=	mass of an ion, au
a_l	=	index for type-l neutral atoms
C	=	capacitor of electrical circuit for a slab, F/m
C_s	=	sound speed
C_α	=	carbon fraction of polyethylene molecule
c_P	=	specific heat at constant pressure
D_c	=	slab capillary gap
D_{tbl}	=	thickness of the transition boundary layer
d	=	width of the initial wall temperature distribution
E	=	magnitude of electrical field
e	=	electron charge
end	=	index denoting condition at the exit plane
F_{rad}	=	radiation heat flux incident on the transition boundary layer
H_α	=	hydrogen fraction of polyethylene molecule
H_w	=	thickness of the capillary wall
h_{CH}	=	enthalpy of a CH-molecule to bring it from the capillary wall to the plasma volume
I	=	discharge current per unit of slab length
i_k	=	index for type-k ions
k_B	=	Boltzmann constant
L	=	inductor of electrical circuit for a slab, H · m
L_c	=	capillary length
M_C	=	mass of a carbon atom, au
M_H	=	mass of a hydrogen atom, au
M_0	=	unit of atomic mass
m_e	=	electron mass
$\hat{n}$	=	normalized gas number density, a variable of the Knudsen layer model
n_a	=	number density of neutral atoms
n_{CH}	=	molecular number density of ablated molecules
n_e	=	electron number density
n_i	=	ion number density
P	=	pressure
Q	=	charge of capacitor for a slab, Q/m
R	=	resistor of electrical circuit for a slab, Ω · m
R_{plasma}	=	plasma resistance for a slab, Ω · m
sat	=	index denoting vapor equilibrium (saturation) conditions
sur	=	index denoting conditions for ablative wall surface
T	=	plasma temperature
T_b	=	maximal wall surface temperature
T_{sur}	=	temperature of the ablative surface
T_w	=	wall temperature
t	=	time
$\hat{u}$	=	normalized directed velocity, a variable of the Knudsen layer model
V_T	=	thermal gas velocity
$\hat{V}$	=	normalized thermal velocity, a variable of the Knudsen layer model
x	=	axis directed across the slab
y	=	axis directed along the slab
z	=	axis directed along the capillary
Z	=	average ion charge state
β	=	ratio of thermal pressure to magnetic pressure
$\hat{\beta}$	=	variable of the Knudsen layer model
Γ_{CH}	=	molecular ablation/absorption rate
$\Gamma_{\text{CH,max}}$	=	maximal molecular ablation rate
γ	=	ratio of specific heats
ΔD_c	=	change of slab capillary gap
$\Delta\varepsilon_\Phi$	=	sum of vaporization, dissociation, ionization and electronic excitation energies per CH molecule
ε_{CH}	=	internal plasma energy per CH molecule
η	=	radiation absorption length of the wall material
Θ	=	energy flux incoming into the capillary wall
κ_w	=	wall material specific heat
λ_{rad}	=	plasma radiation absorption length
ν_{ea}	=	collision frequency between electrons and neutral atoms
ν_{ei}	=	collision frequency between electrons and ions

Presented as Paper 2009-3736 at the 40th AIAA Plasmadynamics and Laser Conference, San Antonio, TX, 22–25 June 2009; received 16 February 2010; revision received 16 September 2010; accepted for publication 17 September 2010.

*Research Scientist; leonid.pekker.ctr@edwards.af.mil.
†Contractor; oksana.pekker@gmail.com.

Π = radiation heat source in the bulk of capillary wall
ρ_w = wall material mass density
σ = electrical conductivity
σ_{eC} = electron collision cross section with a neutral carbon atom
σ_{eH} = electron collision cross section with a neutral hydrogen atom
τ = time step
φ = ionization ratio
χ_w = wall thermal conductivity

I. Introduction

THE role of space-based systems for both commercial and government customers continues to evolve, continually providing new requirements for the development of satellite propulsion systems. As it is very thermally efficient (small heat losses through the ablative walls), a high-pressure ($5 \times 10^6 - 5 \times 10^8$ Pa) ablative capillary discharge is a good candidate for high-power (tens of kilowatts) plasma thrusters.

A schematic of a slab capillary discharge thruster is shown in Fig. 1. The discharge maintains a resistive arc through a narrow insulating capillary by the continual ablation of an injected mass or, more commonly, the capillary wall material as shown in Fig. 1. The ablative capillary discharge can be described via a three-layer configuration. The outermost layer is a solid wall, usually some form of polyethylene, occasionally Teflon or some other insulating material. Material from the wall is evaporated, entering the thin transition boundary layer, where it is dissociated, ionized and heated to plasma temperature. The innermost layer is the plasma core. The closed end of the capillary (left side of Fig. 1) is one electrode; the other electrode (right side of Fig. 1) is an open end through which the plasma can flow and expand. Ohmic heating is responsible for plasma heating, ionization, ablation, and radiation. In the model, the sonic condition ($Ma = 1$ in Fig. 1) is assumed to exist at the open end of the capillary.

As it has been mentioned in [1], in terms of plasma propulsion concepts, the thermal capillary plasma thruster must satisfy two main conditions. First, the capillary plasma should be in a local thermodynamic equilibrium (LTE), indicating that the electrons, ions, and neutrals have the same temperature. Then, the electrical current will heat both the electrons and the heavy particles (i.e., not only the electrons), which gives a smaller I_{sp} than in the case of heating only electrons at the same input power, thus providing high thrust per watt. Second, as it is well known, pinching the capillary discharge due to the magnetic field generated by the discharge current, leads to a formation of a narrow plasma core region with a high electron temperature and a large, relatively cold peripheral plasma region. This also decreases the efficiency of the capillary thruster, because only a small amount of input discharge energy is transferred to the heavy particles and almost all of the input energy is transferred to the electrons. To minimize the pinching of the capillary discharge, the ratio of the thermal pressure to the magnetic pressure, β, in the capillary plasma thruster should be greater than unity.

The first paper to discuss the use of ablative capillary discharge for propulsion was published in the United States in 1982 [2]. In it, the authors introduced their concept of the pulsed electrothermal thruster; this group later built and tested such devices [3,4]. Since then many theoretical papers have been published exploring the applications of such discharges to electrothermal capillary thrusters, electrothermal launchers, and electrothermal chemical guns; a review of these papers with the corresponding references can be found in a recent theoretical paper [1]. It should be noted that in [1] the author for the first time used a radiation heat transfer model based on a radiation database. This database was constructed using PrismSPECT,[‡] a radiation software that calculates the radiation spectrum output from a uniform plasma slab. Thus, unlike earlier models, this model does not use any asymptotic radiation models, such as blackbody radiation models with a gray factor or volumetric bremsstrahlung (free–free) radiation model, but self-consistently calculates the radiation heat flux at the transition boundary layer, Fig. 1. However, the model [1] neglects the radiation and thermal conduction heating of the bulk capillary wall, assuming that all radiation entering the transition boundary layer is absorbed into this region and expended on the ablation of wall material. On the other hand, as it has been indicated in works [5–7] the heat losses in the capillary wall, can play a noticeable role in heat transfer of relatively high-pressure ($2 \cdot 10^5 - 2 \cdot 10^6$ Pa) capillary discharges. Therefore, extending model [1] to the case including heat transfer in the capillary wall is important to better understand the physics of high-pressure ablative capillary discharge and engineering aspects of the capillary discharge thrusters.

The present paper extends the model [1] to the case including heat transfer in the bulk of capillary wall by taking into account the capillary wall thermal conduction and radiation wall absorption. A description of the model and numerical results are presented in Secs. II and III, respectively, and conclusions are given in Sec. IV.

II. Description of the Model

The following sections describe the assumptions and the model.

A. Assumptions

The following assumptions are made in the model:

1) The boundary transition layer, Fig. 1, is assumed to be thin with respect to the capillary gap, and is treated in the model as the interface between the plasma core and the capillary wall. This assumption is based on the premise that the radiation heat transfer across the capillary is so strong that it flattens the temperature and density distributions across the plasma core, leading to a very thin transition boundary layer. Unfortunately, there exists no model of the ablative capillary discharge that would verify this premise. The main challenge for constructing such a model is a comprehensive description of the heat transfer across the capillary discharge. However, experimental observations [8,9] do not seem to contradict this assumption.

2) The temperatures of electrons and heavy particles (ions and neutrals) are equal, that is, LTE condition is achieved.

3) The temperature of the ablative gas entering the plasma core region from the transition boundary layer, Fig. 1, is equal to T, the average temperature of the capillary plasma. In other words, the plasma radiation ablates the capillary wall, then dissociates and ionizes ablated gas, and finally heats it to the plasma temperature in the thin transition boundary layer, as shown in Fig. 2. In this figure, a polyethylene molecule from the capillary wall enters the transition layer (a) and becomes dissociated and ionized at the boundary between the transition layer and the plasma (b). This assumption has been made in all previous models (see [1] and references therein) and, as discussed above, can be verified only in a model that would include radiation heat transfer across the capillary.

4) The magnetic pressure is much smaller than the thermal pressure, that is, $\beta \gg 1$.

5) Plasma composition can be calculated using the Saha equation, that is, local ionization equilibrium is achieved.

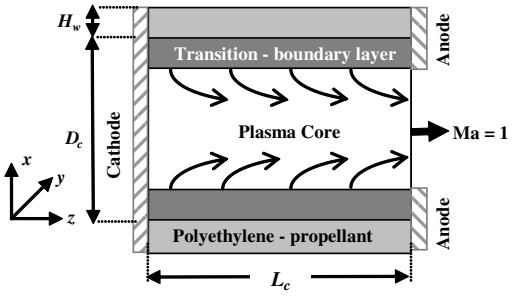

Fig. 1 Schematic (not to scale) of slab capillary discharge operation; (z, x) cross section is shown.

[‡]Prism Computational Sciences, Inc., 455 Science Drive, Suite 140, Madison, WI 53711.

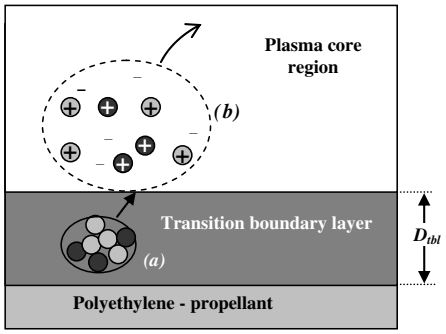

Fig. 2 Schematic of capillary discharge (not to scale) showing the transition boundary layer between the solid wall and the plasma.

6) The conduction heat flux in the plasma core region is much smaller than the radiation flux at the inner boundary of the transition boundary layer and can be ignored.

7) Heating of the plasma by the viscous dissipation is small and can be omitted.

8) The gas in the plasma core region and in the transition boundary layer is fully dissociated. As shown in [1], assumptions 2, 4–8 are well satisfied in ablative high-pressure capillary discharges.

9) A sonic condition ($Ma = 1$ in Fig. 1) exists at the open end of the capillary.

10) The capillary wall is polyethylene, C_4H_9.

11) The capillary is a 4 mm slab. All 11 of these assumptions have been analyzed in detail in [1].

12) Unlike in [1], where the heat losses into the capillary wall were neglected, this paper takes them into account. We assume that the capillary wall radiation absorption length η is a constant, independent of wavelength and wall temperature; model [1] corresponds to the case where $\eta = 0$. This assumption is actually not accurate because the extinction coefficient of polyethylene depends considerably on wavelength [10,11] (at room temperature it varies from 10^{-5} to 1 in the region 0.02–0.3 microns, where the main part of plasma radiation spectrum is located) and temperature. However, because our model is not capable of calculating the radiation spectrum at the capillary wall anyway, and, to the best of our knowledge currently there is no experimental or theoretical data on optical properties of polyethylene as a function of temperature, we have used η as an input parameter.

13) The thermal conductivity of polyethylene is a constant, independent of temperature. In the model, all properties of polyethylene at room temperature have been taken from a handbook.

In our model we use the radiation-plasma-composition database [1]. This database was constructed using PrismSPECT software for C_4H_9 capillary wall composition and described in detail in [1].

B. Basic Equations

The equations describing mass and energy conservation laws in the plasma core region of a slab capillary discharge, Fig. 1, can be written as

$$D_c \cdot L_c \cdot \frac{\mathrm{d}n_{\mathrm{CH}}}{\mathrm{d}t} = 2 \cdot L_c \cdot \Gamma_{\mathrm{CH}} - D_c \cdot n_{\mathrm{CH,end}} \cdot C_{s,\mathrm{end}} \tag{1}$$

$$D_c \cdot L_c \cdot \frac{\mathrm{d}(n_{\mathrm{CH}} \cdot \varepsilon_{\mathrm{CH}})}{\mathrm{d}t} = \frac{I^2 \cdot L_c}{D_c \cdot \sigma(n_{\mathrm{CH}}, T)} - D_c \cdot n_{\mathrm{CH,end}} \cdot C_{s,\mathrm{end}} \cdot h_{\mathrm{CH}} - 2 \cdot L_c \cdot \Theta \tag{2}$$

where

$$\Theta = \begin{cases} (F_{\mathrm{rad}} - \Gamma_{\mathrm{CH}} \cdot h_{\mathrm{CH}}) & \text{if } F_{\mathrm{rad}} > \Gamma_{\mathrm{CH}} \cdot h_{\mathrm{CH}} \\ 0 & \text{if } F_{\mathrm{rad}} < \Gamma_{\mathrm{CH}} \cdot h_{\mathrm{CH}} \end{cases} \tag{3}$$

$$h_{\mathrm{CH}} = \Delta\varepsilon_{\Phi} + c_P \cdot k_B \cdot T \cdot (1 + Z \cdot \varphi) \cdot (C_\alpha + H_\alpha) \tag{4}$$

$$h_{\mathrm{CH}} - \varepsilon_{\mathrm{CH}} = k_B \cdot T \cdot (1 + Z \cdot \varphi) \cdot (C_\alpha + H_\alpha) \tag{5}$$

$$n_{\mathrm{CH,end}} = n_{\mathrm{CH}} \cdot \left(\frac{2}{\gamma + 1}\right)^{1/(\gamma-1)}, \qquad T_{\mathrm{end}} = \left(\frac{2}{\gamma + 1}\right) \cdot T \tag{6}$$

$$C_{s,\mathrm{end}} = \left[\frac{\gamma \cdot k_B \cdot T_{\mathrm{end}} \cdot (1 + Z_{\mathrm{end}} \cdot \varphi_{\mathrm{end}})}{A \cdot M_0}\right]^{1/2}$$
$$\sigma = \frac{n_e \cdot e^2}{m_e \cdot (\nu_{ea} + \nu_{ei})}, \qquad A = \left(\frac{C_\alpha \cdot M_C + H_\alpha \cdot M_H}{C_\alpha + H_\alpha}\right) \tag{7}$$

$C_\alpha = 4, H_\alpha = 9, \gamma = 5/3, c_P = \gamma/(\gamma - 1)$, and $\varphi = n_i/(n_i + n_a)$ is the ionization ratio; the vaporization and dissociation energies are considered constants in the model and input parameters in the code. For the electron-ion momentum transfer collision frequency, ν_{ei}, we use the Spitzer equation [12] modified by Zollweg and Liebermann [13] to account for nonideal effects due to high density of the plasma, and for the electron-neutral momentum transfer collision frequency, ν_{ea}, we use the electron-neutral collision cross sections [9], $\sigma_{eC} = 2.64 \cdot 10^{-19}$ m^2 and $\sigma_{eH} = 1.49 \cdot 10^{-19}$ m^2; for more details see [1]. In the model, we use a radiation-plasma-composition database [1] that has been constructed using PrismSPECT software. Applying a standard linear-interpolation method to the database, we calculate the radiation heat flux incident on the transition boundary layer, F_{rad}, and the plasma composition for a given plasma temperature and total number density of heavy particles (neutrals and ions). The index "end" denotes conditions at the exit plane, while the absence of this index denotes conditions averaged over the volume of the capillary. In the model, to connect the plasma parameters in the bulk of capillary with the parameters of the plasma jet at the exit plane, we use isentropic flow relations [14] in a small region $\sim D_c$ at the exit plane, where the plasma is accelerated up to the speed of sound. Because in this gas-accelerated-region the heat losses at the wall and heating of the gas (by the current) are much smaller than the total enthalpy of gas flow, using isentropic flow relations in this region are reasonable. We also assume that the average ion charge and ionization ratio are preserved through this region, $Z_{\mathrm{end}} = Z$, and $\varphi_{\mathrm{end}} = \varphi$ [1].

In the mass conservation equation, Eq. (1), the first term on the right-hand side describes the number of CH-polyethylene molecules arriving at the plasma core region from the ablative surface per unit of time and per unit of the slab length in the y-direction, Fig. 1, as illustrated in Fig. 2, where a polyethylene molecule from the capillary wall enters the transition layer (a) and becomes dissociated and ionized at the boundary between the transition layer and the plasma (b). The second term represents the flow of CH-polyethylene molecules leaving the capillary chamber through the open capillary end per unit of the slab length in the y-direction. The factor of 2 in the first term of Eq. (1) corresponds to the two capillary walls in slab geometry. It is worth noting, that the case of $\Gamma_{\mathrm{CH}} < 0$ corresponds to the plasma decay case where the particles are absorbed by the capillary wall (not ablated from the wall). In the energy conservation Eq. (2), the first term on the right-hand side represents Ohmic heating of the plasma, the second term represents the enthalpy flow leaving the capillary with the plasma jet through the open capillary end, and the third term represents energy losses in the bulk of the capillary wall. It should be stressed that we assume that the heat flux can be directed only from the plasma to the wall, Eq. (3). This has a perfect physical explanation: in high-pressure capillary discharges the temperature of the plasma core region is always larger than the temperature of the polyethylene capillary which is usually much less than 0.1 eV. As one can see, taking $\Theta = 0$, i.e., no heat losses in the bulk of the capillary wall, we recover the model from [1].

The heat transfer in the bulk of the capillary wall can be written as

$$\kappa_w \cdot \rho_w \cdot \frac{\partial T_w}{\partial t} - \chi_w \cdot \frac{\partial^2 T_w}{\partial x^2} = \Pi \tag{8}$$

where Π is the radiation heat source in the bulk of capillary wall

$$\Pi = \begin{cases} (1/\eta)\cdot\exp(-x/\eta)\cdot(F_{\text{rad}}-\Gamma_{\text{CH}}\cdot h_{\text{CH}}) & \text{if } (F_{\text{rad}}>\Gamma_{\text{CH}}\cdot h_{\text{CH}}) \text{ and } (\Gamma_{\text{CH}}>0) \\ (1/\eta)\cdot\exp(-x/\eta)\cdot F_{\text{rad}} & \text{if } (\Gamma_{\text{CH}}<0) \\ 0 & \text{if } (F_{\text{rad}}>\Gamma_{\text{CH}}\cdot h_{\text{CH}}) \end{cases} \tag{9}$$

The first case in Eq. (9) corresponds to the case of the wall ablation process, where the radiation flux in the bulk of the capillary wall is given by $\exp(-x/\eta)\cdot(F_{\text{rad}}-\Gamma_{\text{CH}}\cdot h_{\text{CH}})$. In this case the radiation leaving the plasma core region, F_{rad}, ablates the capillary wall, dissociates, ionizes, and heats the ablative vapor up to the plasma temperature in the transition boundary (which leads to its decrease for the $\Gamma_{\text{CH}}\cdot h_{\text{CH}}$ amount); it is then absorbed in the bulk of capillary wall; and, finally, it leaves the capillary. The second case corresponds to the plasma decay process, where the mass flux is directed from the plasma core to the capillary wall. In this process all the plasma radiation, F_{rad}, is absorbed by the bulk of capillary wall or leaves the capillary; the enthalpy flux of particles, $\Gamma_{\text{CH}}\cdot h_{\text{CH}}$, is absorbed by the capillary wall surface and should be taken into account in the boundary conditions at the inner surface of the capillary wall. The third case in Eq. (9) corresponds to the situation where all radiation coming into the transition boundary layer from the plasma core region is completely absorbed into it, the case of no heat losses in the bulk of the capillary wall.

It should be stressed that, although in our model we do calculate the change in the slab gap vs time, ΔD_c, during the discharge pulse, we neglect this in our radiation database, where D_c is assumed to be constant and cannot be varied. This approximation is acceptable until $\Delta D_c \ll D_c$. In our calculations, ΔD_c was only about a few microns, while D_c was 4 mm. However, for long pulse discharges, the effect of changing the capillary gap due to ablation has to be taken into account in the radiation database.

In the model we employed a resistor-inductor-capacitor circuit, Fig. 3, to self-consistently calculate the parameters of the capillary discharge and the temperature distribution in the capillary walls vs time. The equation describing the circuit can be written as

$$\frac{Q}{C} = -L\cdot\frac{\mathrm{d}^2Q}{\mathrm{d}t^2} - (R_{\text{plasma}}+R)\cdot\frac{\mathrm{d}Q}{\mathrm{d}t} \tag{10}$$

The initial parameters for this circuit are initial capacitor voltage and initial circuit current $I=-\mathrm{d}Q/\mathrm{d}t$.

C. Boundary Conditions

Boundary conditions connecting the plasma core parameters with the parameters at the ablative surface are as follows:

$$\Gamma_{\text{CH}} = n_{\text{CH,sat}}(T_{\text{sur}})\cdot V_{T,\text{sur}}\hat{n}\cdot\hat{u} \tag{11}$$

$$P(n_{\text{CH}},T) = P_{\text{sat}}(T_{\text{sur}})\cdot\hat{n}\left(\frac{\hat{V}^2}{2}+\hat{u}^2\right) \tag{12}$$

$$\frac{1}{2\cdot\sqrt{\pi}} = \hat{n}\cdot\hat{u}\left(1+\hat{\beta}\cdot\left[\frac{\hat{u}}{2}\cdot erfc\left(\frac{\hat{u}}{\hat{V}}\right)-\frac{\hat{V}}{2\cdot\sqrt{\pi}}\exp\left(-\frac{\hat{u}^2}{\hat{V}^2}\right)\right]\right) \tag{13}$$

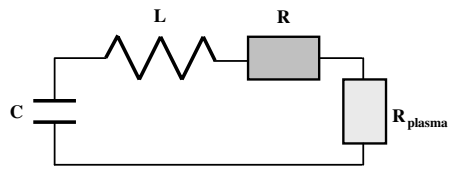

Fig. 3 RLC circuit for modeling capillary discharge.

$$\frac{1}{4} = \hat{n}\cdot\left(\frac{\hat{V}^2}{2}+\hat{u}^2\right)-\hat{n}\cdot\hat{\beta}\cdot\left(\left[\frac{\hat{u}^2}{2}+\frac{\hat{V}^2}{4}\right]\cdot erfc\left(\frac{\hat{u}}{\hat{V}}\right)-\frac{\hat{V}\cdot\hat{u}}{2\cdot\sqrt{\pi}}\cdot\exp\left(\frac{\hat{u}^2}{\hat{V}^2}\right)\right) \tag{14}$$

$$\frac{1}{\sqrt{\pi}} = \hat{n}\cdot\hat{u}\cdot\left(\frac{5\cdot\hat{V}^2}{2}+\hat{u}^2\right)-\hat{n}\cdot\hat{\beta}\cdot\hat{V}^3\cdot\left(\frac{1}{2\cdot\sqrt{\pi}}\cdot\left[\frac{\hat{u}^2}{\hat{V}^2}+2\right]\cdot\exp\left(-\frac{\hat{u}^2}{\hat{V}^2}\right)-\frac{\hat{u}}{2\cdot\hat{V}}\cdot\left(\frac{5}{2}+\frac{\hat{u}^2}{\hat{V}^2}\right)erfc\left(\frac{\hat{u}}{\hat{V}}\right)\right) \tag{15}$$

where Eq. (11) calculates the flux of the ablative polyethylene molecules; Eq. (12) states that the pressure in the plasma core is equal to the vapor pressure in the Knudsen layer at the ablative surface (the Knudsen layer is a part of the transition layer); and Eqs. (13–15) describe the Knudsen layer at the ablative surface using Anisimov's velocity distribution function [15]; here we have adopted the Knudsen layer model [16]. Here $\hat{u}$ and $\hat{V}$ are the directed and thermal vapor velocities at the outer boundary of the Knudsen layer, normalized by the equilibrium vapor thermal velocity, $V_{T,\text{sur}}$; $\hat{n}$ is the vapor number density at the outer boundary of the Knudsen layer, normalized by the equilibrium vapor number density, $n_{\text{CH,sat}}$; and $\hat{\beta}$ is a parameter of the Knudsen layer model [16] describing the backscattering flux of the molecules at the ablative surface. In the case of thermodynamic equilibrium $\hat{u}=\hat{V}=\hat{\beta}=1$. As one can see, solving Eqs. (11–15) at the given P, P_{sat}, and $V_{T,\text{sur}}$ allows us to calculate the values of $\hat{u}$, $\hat{n}$, $\hat{V}$, $\hat{\beta}$, and Γ_{CH}. In the model we use the following expressions for the equilibrium polyethylene vapor pressure P_{sat} [6], thermal velocity of the evaporated atoms $V_{T,\text{sur}}$, and density $n_{\text{CH,sat}}$

$$P_{\text{sat}} = \exp\left[5565.22\cdot\left(\frac{1}{453}-\frac{1}{T_{\text{sur}}}\right)\right] \tag{16}$$

$$V_{T,\text{sur}} = \sqrt{\frac{2\cdot k_B\cdot T_{\text{sur}}}{M_0\cdot A}} \tag{17}$$

$$n_{\text{CH,sat}} = \frac{P_{\text{sat}}}{k_B\cdot T_{\text{sur}}\cdot(C_\alpha+H_\alpha)} \tag{18}$$

In Eq. (18) we have assumed that all vapor leaving the ablative surface is fully dissociated. It is worth noting that in this Knudsen layer model, we ignore the thermal conductivity in the Knudsen layer, assuming that radiation heat flux at the ablative surface is much larger than thermal conduction [17]. Indeed, because in the model we assume that the radiation heat flux at the inner boundary of the transition layer is much larger than the conduction heat flux in the plasma core region (assumption 6) the conduction heat flux in the Knudsen is small and can be dropped from the consideration.

Boundary conditions at the outer and inner boundaries of the capillary walls are

$$\left.\frac{\partial T_w}{\partial x}\right|_{H_w} = 0 \tag{19}$$

$$\begin{cases} \left.\frac{\partial T_w}{\partial x}\right|_{x_{\text{sur}}} = 0 & \text{if } (\Theta>0) \text{ and } (\Gamma_{\text{CH}}>0) \\ \left.\frac{\partial T_w}{\partial x}\right|_{x_{\text{sur}}} = \frac{\Gamma_{\text{CH}}\cdot h_{\text{CH}}}{\chi_w} & \text{if } (\Theta>0) \text{ and } (\Gamma_{\text{CH}}<0) \\ T_{\text{sur}} = T_b & \text{if } \Theta=0 \end{cases} \tag{20}$$

where $x_{\text{sur}}=0$ and $x=H_w$ are the coordinates of the inner and outer boundaries of the capillary walls. Equation (19) specifies no conduction heat flux at the outer boundary of the capillary wall. The

first case in Eq. (20) specifies no conduction heat flux at the inner boundary of the capillary wall in the wall ablation regime. The second case corresponds to the absorption wall regime, the regime in which the mass flux is directed from the plasma to the capillary walls. In this regime the incident particles bring their enthalpy to the capillary wall surface, inducing the corresponding conduction heat flux at the capillary wall. The third case specifies the surface wall temperature as a maximum wall temperature T_b that can provide the maximum ablation rate due to radiation:

$$\Gamma_{\mathrm{CH,max}} = \frac{F_{\mathrm{rad}}}{h_{\mathrm{CH}}} \tag{21}$$

Thus, Eq. (20) as well as Eqs. (3) and (9), state that heat flux can be directed only from the plasma to the wall, and therefore

$$\Gamma_{\mathrm{CH}} \le \Gamma_{\mathrm{CH,max}} \tag{22}$$

D. Algorithm

Let us now describe the algorithm for calculating capillary discharge parameters and the temperature distribution in the capillary wall. The algorithm consists of the following major steps:

1) Assume initial values of n_{CH}, and T, and $T_w(x)$, I, and Q.

2) Calculate all plasma parameters for given n_{CH}, and T.

3) Calculate $\Gamma_{\mathrm{CH,max}}$ using Eq. (21).

4) Calculate the maximum allowed wall surface temperature T_b by substituting $\Gamma_{\mathrm{CH,max}}$ and $P(n_{\mathrm{CH}}, T)$ into the system of Eqs. (11–15).

5) Calculate Γ_{CH} by substituting $P(n_{\mathrm{CH}}, T)$ and $T_w(x_{\mathrm{sur}})$ into the system of Eqs. (11–15).

6) Determine the boundary conditions at $x = x_{\mathrm{sur}}$, Eq. (20): 6a) if $(T_w(x_{\mathrm{sur}}) < T_b)$ and $(\Gamma_{\mathrm{CH}} > 0)$ then apply case 1; 6b) if $(T_w(x_{\mathrm{sur}}) < T_b)$ and $(\Gamma_{\mathrm{CH}} < 0)$ then apply case 2; 6c) if $T_w(x_{\mathrm{sur}}) > T_b$ then apply case 3 and set Γ_{CH} equal to $\Gamma_{\mathrm{CH,max}}$.

7) Calculate new time: $t = t + \tau$, where t is the initial time and τ is the time step.

8) Calculate new n_{CH}, and T by solving Eqs. (1) and (2):

$$n_{\mathrm{CH}}^{t+\tau} = n_{\mathrm{CH}}^{t} + \tau \cdot \left[\frac{2 \cdot \Gamma_{\mathrm{CH}}}{D_c} - \frac{n_{\mathrm{CH,end}} \cdot C_{s,\mathrm{end}}}{L_c} \right]^{t} \tag{23}$$

$$n_{\mathrm{CH}}^{t+\tau} \cdot \varepsilon_{\mathrm{CH}}(n_{\mathrm{CH}}^{t+\tau}, T^{t+\tau}) = n_{\mathrm{CH}}^{t} \cdot \varepsilon_{\mathrm{CH}}(n_{\mathrm{CH}}^{t}, T^{t}) + \tau \cdot \left[\frac{I^2}{D_a^2 \cdot \sigma(n_{\mathrm{CH}}, T)} - \frac{n_{\mathrm{CH,end}} \cdot C_{s,\mathrm{end}} \cdot h_{\mathrm{CH}}}{L_c} - 2 \cdot \Theta \right]^{t} \tag{24}$$

9) Calculate new $T_w(x)$ by solving Eq. (8) with boundary conditions (20).

10) Calculate new Q and I solving Eq. (10):

$$Q^{t+\tau} = Q^{t} - I^{t} \cdot \tau \tag{25}$$

$$I^{t+\tau} = I^{t} \cdot \left(1 - \tau \cdot \frac{(R_{\mathrm{plasma}} + R)}{L} \right) + \tau \cdot \frac{Q^{t}}{C \cdot L} \tag{26}$$

11) Go to step 1.

In this work, we have used Bisection Method to solve Eq. (24) and the system of Eqs. (11–15); a standard implicit scheme to solve Eq. (8); and a nonuniform geometric-progression grid.

III. Numerical Results

In the numerical results presented in this section, the combined energy of evaporation and dissociation was taken as 50 eV per C_4H_9 polyethylene molecule, the capillary length was chosen as 8 cm, D_c was 4 mm, the parameters of circuit were $L = 4.661 \cdot 10^{-8}$ H · m, $R = 1.4546\ \Omega \cdot$ m, $C = 1.7507$ F/m, Fig. 3, the initial voltage on the capacitor and the initial discharge current were 2500 V and $1.496 \cdot 10^5$ A/m, respectively. The initial temperature distribution of the wall was chosen as

$$T_w(x) = (527.56 - 300.0) \cdot \frac{\exp[-(x/\eta)^2]}{1 - \exp[-(H_w/\eta)^2]} + \frac{300.0 - 527.56 \cdot \exp[-(H_w/\eta)^2]}{1 - \exp[-(H_w/\eta)^2]} \tag{27}$$

where $x = 0$ corresponds to the ablative surface, $x = H_w$ to the outer boundary of the capillary wall, and the initial parameters of the plasma core were chosen as $n_{\mathrm{CH}} = 1.714 \cdot 10^{23}$ m^{-3}. $T =$ 1.2555 eV, and $I = 1.496 \cdot 10^5$ A/m. Thus, in our calculations, the width of the initial wall temperature distribution, d, is on the order of the radiation absorption length of the wall material which has a perfect physical sense: the larger the η, the more deeply the radiation goes into the capillary wall, heating it; with an increase in x, the wall temperature smoothly decreases down to room temperature at $x = H_w$. The initial wall surface temperature has been chosen as 527.56 K. For smaller wall surface temperatures, we obtained unstable solutions at $\eta = 0.5$ mm; the evaporation rate of the wall material was too low, leading to a sharp increase in the plasma temperature (due to the high rate of Ohmic plasma heating), which very quickly went beyond the maximum plasma temperature allowed by our database. Since our model is not capable of describing the ignition process in capillary discharges anyway, where plasma is far from local thermodynamic equilibrium, we can only guess about initial plasma density, plasma temperature, and parameters of the wall temperature distribution function that we have to use in our model. However, it should be stressed that with time, when the capillary plasma is well developed, the effect of the initial conditions becomes less and less pronounced, and the parameters of the discharge and the wall temperature distribution becomes better and better self-balanced. To investigate how the radiation absorption of the wall affects the capillary discharge, we performed calculations for $\eta = 0.02$, 0.1, and 0.5 mm. It is worth noting, that the selected initial n_{CH}, T, and I correspond to the parameters of the steady-state capillary discharge [1] with no heat losses in the bulk of the capillary walls. We have chosen these conditions to avoid a large unbalance between initial current, plasma temperature, and plasma density; significant unbalance in the initial conditions leads to unstable solutions and the termination of the computational runs.

Figures 4 and 5 show the distributions of β and the LTE-factor [1]

$$K_{\mathrm{LTE}_{e\&Ir;=>i,a}} = k_B \cdot T \cdot \left(\frac{2 \cdot m_e^2}{e^2 \cdot E^2 \cdot M_0} \right) \cdot \left(\sum_k \nu_{ei_k} + \sum_l \nu_{ea_l} \right) \cdot \left[\sum_k (\nu_{ei_k} \cdot (A_{i_k})^{-1}) + \sum_l (\nu_{ea_l} \cdot (A_{a_l})^{-1}) \right] \tag{28}$$

which is the ratio of the average exchange energy between the electrons and the heavy particles, due to their collisions, to the average energy that an electron gains from the electric field between collisions, vs time for different η. In Eq. (28), index k corresponds to the ions of type k, and index l corresponds to the neutrals of type l. As one can see, the LTE-factor and β are much larger than 1; meaning that assumptions 2 and 4 are well satisfied in our calculations. It should be stressed that in Eq. (28) we have ignored inelastic collisions, assuming that inelastic collisions are less important than

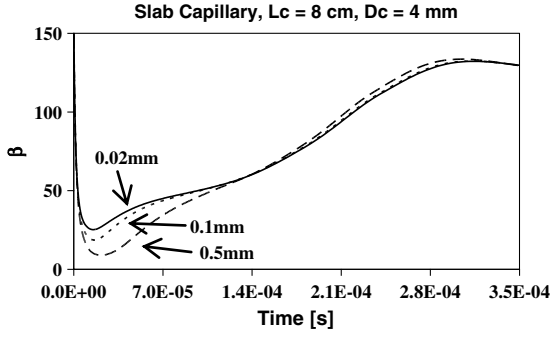

Fig. 4 Ratio of thermal pressure to magnetic pressure for different η.

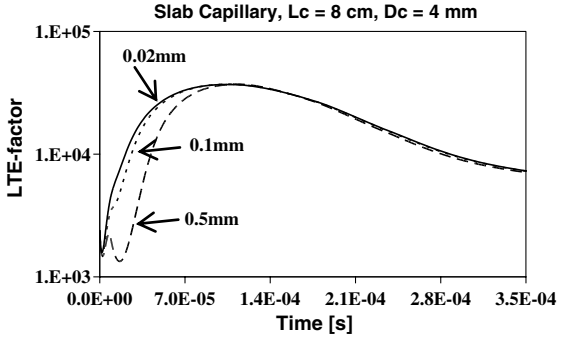

Fig. 5 LTE-factor for different η.

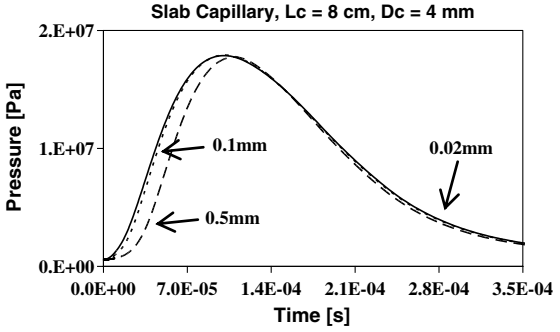

Fig. 8 Plasma pressure for different η.

elastic collisions. However, this is not always the case; the inelastic collisions can play an important role in the determination of the electron temperature. Because the inelastic collisions lead to a significant decrease in the average energy that an electron gains from the electric field between collisions [electrons are losing their energy inelasticly, which has not been taken into account in Eq. (28)], while the energy transferred to the heavy particles in these collisions is about the same as in elastic collisions, we may conclude that Eq. (28) underestimates the LTE-factor. In the model we have also checked assumptions 5–7, employing the methods in [1]; they were also well satisfied in our calculations.

Now let us analyze Figs. 6–11. It is obvious that as the radiation wall absorption length η increases, the temperature of the ablative surface decreases, as shown at the positive slopes of T_{sur} in Fig. 6, leading to a smaller vaporization rate of the wall material. This results in smaller plasma densities and a correspondingly smaller plasma pressure for larger η, as shown in Figs. 7 and 8, but in larger plasma temperatures due to the Ohmic plasma heating (Fig. 9). On the other hand, because of the highly nonlinear dependence of the plasma electrical resistivity on the plasma temperature and plasma composition, the discharge current does not exhibit a significant dependence on η, as shown in Fig. 10; however, it is clear that with an increase in η, the peak current rises. The dip in n_{CH} and the peak in T at the early stage of the discharge seen in Figs. 7 and 9 can be explained by a large imbalance between the ablation, rapid Ohmic heating, and plasma exhaust through the open capillary end at the initial stage of the capillary discharge development; the characteristic time of this stage can be estimated as a few L_c/C_s, which translates to about 20–30 microseconds in our case, Figs. 7 and 9.

From the moment in time when the surface temperature reaches maximum and begins to fall, Fig. 6, all parameters of the discharge become weakly dependent on η, as seen in Figs. 4–10. This observation can be explained by the fact that when T_{sur} decreases

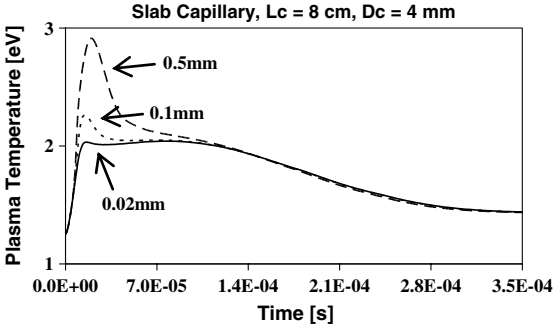

Fig. 9 Plasma temperature for different η.

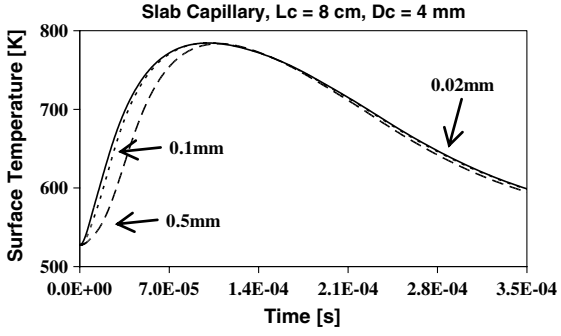

Fig. 6 Temperature of ablative surface for different η.

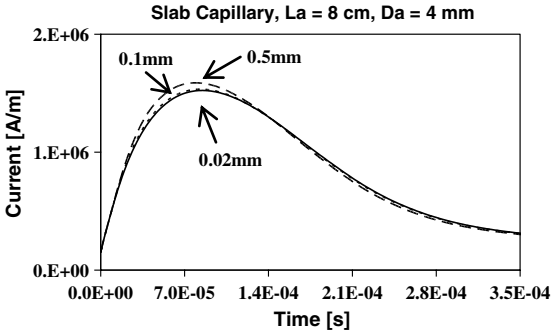

Fig. 10 Discharge current for different η.

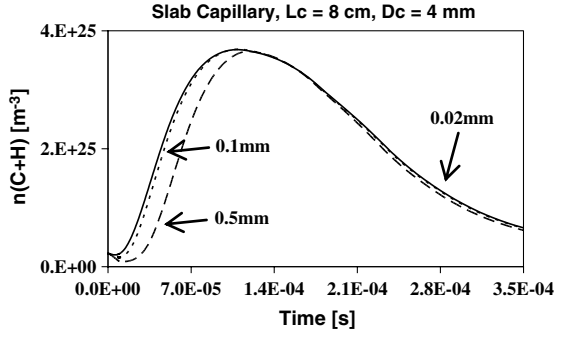

Fig. 7 Number density of heavy particles for different η.

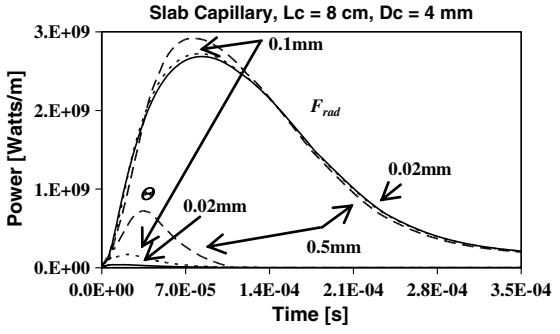

Fig. 11 F_{rad} and Θ for different η.

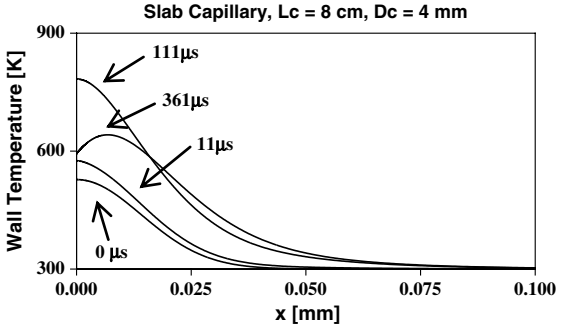

Fig. 12 Wall temperature distribution for $\eta = 0.02$ mm at different moments of time.

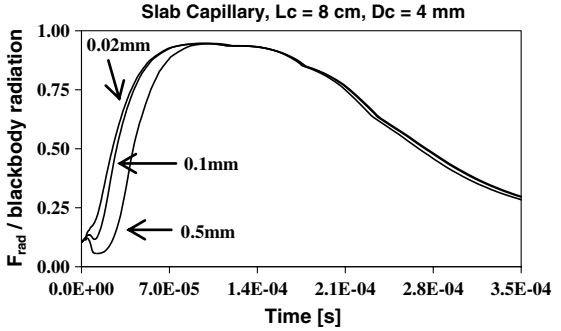

Fig. 15 Grey factor for different η.

with time, the heat losses in the bulk of the capillary wall approach zero in the model, as seen in Fig. 11, and, therefore, the parameters of the discharge become weakly dependent on η. Figure 11 also demonstrates that the energy losses in the capillary bulk dramatically increase with an increase in the radiation wall absorption length, as of course we expect.

Figures 12–14 illustrate wall temperature distributions at different moments of time and for different η. Since the thermal conductivity of the polyethylene is small, the characteristic widths of the temperature distributions depend on η. However, when the ablative surface is cooled by the vaporization process, the length of the region with a positive temperature slopes depends on χ_w.

Figure 15 shows the ratio of the calculated radiation flux at the transition boundary layer, Fig. 1, to the blackbody radiation flux with the same plasma temperature, that is, the gray factor. As one can see the gray factor varies from 0.06 to 0.95. This illustrates that the gray factor can change significantly with time in a nonsteady operation regime and, therefore, assuming that it is constant can lead to false results.

One of the most important parameters of thruster performance is the thrust efficiency, defined as how much of the energy deposited or stored in the propellant is actually transferred into the kinetic energy of the gas/plasma leaving the rocket. Figure 16 shows the thrust efficiency calculated for the steady-state capillary discharge regime for different capillary lengths. In these calculations we have assumed no heat losses from the capillary walls and the energy of evaporation and dissociation have been taken as zero (for polyethylene they are much smaller than the ionization potential of carbon and hydrogen and because the ionization ratio of the plasma in these stationary regimes are larger than 15% [1] they can be ignored). As shown in Fig. 16, the model gives two steady-state solutions at the given plasma temperature. The first solution corresponds to the superhigh-pressure (SHP) regime [1] in which the plasma is so dense that the plasma radiation absorption length λ_{rad} is less than the slab gap of the capillary. The second regime occurs when the plasma density is much lower, so that $\lambda_{\text{rad}} \gg D_c$, that is the case of moderately high plasma pressure, MHP regime. Detailed discussion of steady-state solutions and results can be found in [1]. As one can see at a given plasma temperature in the SHP regime the thrust efficiency increases with capillary length and in MHP regime decreases. An explanation of this observation as follows.

In high-pressure capillary discharges with plasma temperatures of a few electron volts, the main part of electrical energy deposited in the

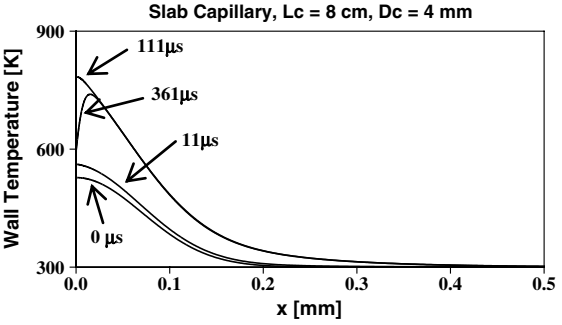

Fig. 13 Wall temperature distribution for $\eta = 0.1$ mm at different moments of time.

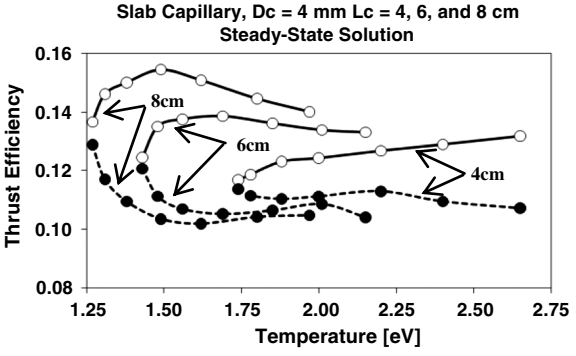

Fig. 16 Thrust efficiency for different L_c; dashed line: MHP regime, solid: SHP regime.

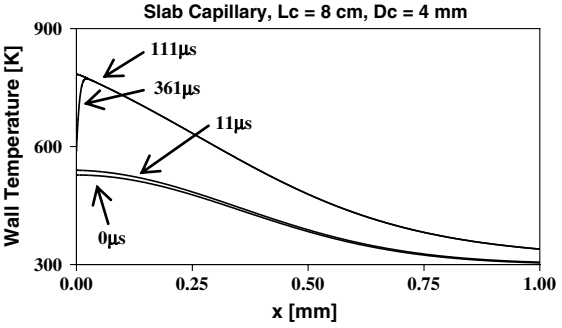

Fig. 14 Wall temperature distribution for $\eta = 0.5$ mm at different moments of time.

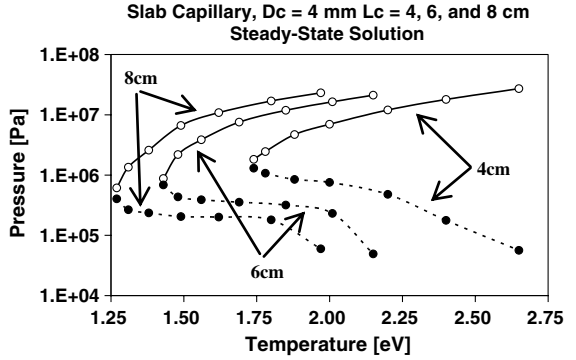

Fig. 17 Plasma Pressure for different L_c; dashed line: MHP regime, solid SHP.

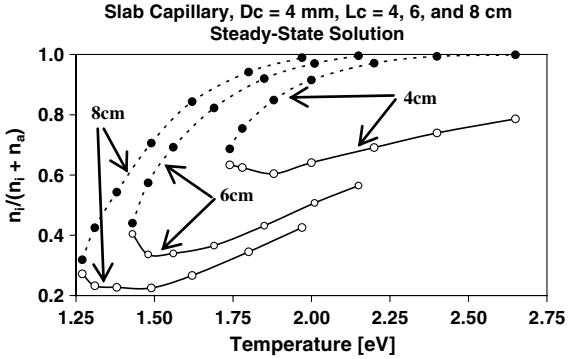

Fig. 18 Ionization ratio for different L_c; dashed line: MHP regime, solid SHP regime.

discharge is spent on ionization of the vapor arriving into the plasma core region, Fig. 1. Because the ionization ratio decreases with an increase in the plasma pressure (this follows from the Saha equation), the ratio of energy contribution in ionization of the vapor arriving in the plasma core region, Fig. 1, to the total energy spent heating the vapor up to plasma temperature decrease with an increase in the plasma pressure. As follows from Figs. 17 and 18, at a given plasma temperature for SHP regime of operation, the plasma pressure increases and correspondingly the ionization ratio decreases with an increase in the capillary length, while the plasma pressure decreases and ionization ratio increases in MHP regimes. Thus, because the main part of enthalpy leaving the capillary with the plasma jet is in ionization, the thrust efficiency decreases with an increase in the ionization ratio corresponding to the trends seen in Fig. 16.

The fact that the main part of plasma enthalpy is in ionization energy, not in thermal energy of the plasma, explains why the thrust efficiency of high-pressure capillary discharge does not exceed 20%, Fig. 16. Using a nozzle may significantly improve the performance of capillary thrusters by conversion of the thermal and chemical energies of the plasma leaving the capillary into kinetic energy of the plasma jet, as in ordinary chemical rockets.

IV. Conclusions

We have presented a zero-dimensional model of high-pressure slab capillary discharge model with capillary wall thermal conduction and radiation absorption. The model includes: a heat-radiation model based on a radiation database to self-consistently calculate the radiation flux at the thin transition boundary layer between the uniform plasma core and the ablative surface; a model of the transition boundary layer to obtain the boundary conditions connecting the plasma core parameters with the parameters at the ablative surface; and the resistor-inductor-capacitor circuit. Thus, the model allows the self-consistent calculation of plasma parameters and distribution of wall temperature vs time. The radiation wall absorption coefficient is assumed to be constant and is an input parameter of the model. The last assumption is actually not accurate because the extinction coefficient of polyethylene is considerably dependent on wavelength and temperature which may change significantly in the course of discharge. Because the model is not capable of calculating the radiation spectrum at the ablative surface anyway, this is the extend of what the model is capable of.

Our model shows that a small extinction coefficient for the wall material leads to a large energy losses from the capillary discharges (the heat is absorbed by the bulk of the capillary wall or just escapes the capillary), and to a spike in the plasma temperature. If the extinction coefficient is too small, the discharge may become extinguished because the temperature of ablative surface does not increase fast enough to compensate the plasma exhaust from the open end of the capillary, Fig. 1. Thus, for thruster applications the capillary wall material has to have a radiation absorption coefficient as large as possible to improve the energy efficiency of the thruster and to more easily achieve stable regimes of thruster operation.

The model also indicates that despite the fact that thrust efficiency of the high-pressure capillary discharge thruster does not exceed 20%, likewise in all thermal thrusters at high temperatures, its performance can be significantly improved by using a nozzle, as in conventional chemical rockets.

Acknowledgments

The authors would like express their gratitude to A. Pekker, M. Kapper, and S. Keith for their kind help in preparing the text of this paper.

References

[1] Pekker, L., "A Zero-Dimensional Time-Dependent Model of High-Pressure Ablative Capillary Discharge for Plasma Thrusters," *Journal of Propulsion and Power*, Vol. 25, No. 4, 2009, pp. 958–969. doi:10.2514/1.41076

[2] Burton, R. L., Goldstein, S. A., Tidman, D. A., and Winsor, N. K., "Theory of the Pulsed Electrothermal Thruster," AIAA Paper 1982-1952, Nov. 1982.

[3] Burton, R. L., Goldstein, S. A., Hilko, B. K., Tidman, D. A., and Winsor, N. K., "Investigation of a Pulsed Electrothermal Thruster," GT Devices, Inc., NASA CR-168266, Oct. 1983.

[4] Burton, R. L., Goldstein, S. A., Hilko, B. K., Tidman, D. A., and Winsor, N. K., "Experimental Investigation of the Pulsed Electrothermal (PET) Thruster," AIAA Paper 1984-1386, June 1984.

[5] Keidar, M., and Boyd, I. D., "Model of an Electrothermal Pulsed Plasma Thruster," *Journal of Propulsion and Power*, Vol. 19, No. 3, 2003, pp. 424–430. doi:10.2514/2.6125

[6] Keidar, M., and Boyd, I. D., "Ablation Study in the Capillary Discharge of an Electrothermal Gun," *Journal of Applied Physics*, Vol. 99, No. 5, 2006, p. 053301. doi:10.1063/1.2174111

[7] Admitsu, T., and Tahara, H., "Experimental and Numerical Study of an Electrothermal Pulsed Thruster for Small Satellites," *Vacuum*, Vol. 80, Nos. 11–12, 2006, pp. 1223–1228. doi:10.1016/j.vacuum.2006.01.055

[8] Loeb, A., and Kaplan, Z., "A Theoretical Model for the Physical Processes in the Confined High Pressure Discharges of Electrothermal Launches," *IEEE Transactions on Magnetics*, Vol. 25, No. 1, 1989, pp. 342–346. doi:10.1109/20.22561

[9] Powell, J. D., and Zielinski, A. E., "Theory and Experiment for an Ablative-Capillary Discharge and Application to Electrothermal-Chemical Gun," U.S. Army Ballistic Research Lab. Rept. BRL-TR-3355, Aberdeen Proving Ground, MD, June 1992.

[10] Painter, L. R., Arakawa, E. T., Williams, M. W., and Ashley, J. C., "Optical Properties of Polyethylene: Measurement and Applications," *Radiation Research*, Vol. 83, No. 11980, pp. 1–18. doi:10.2307/3575254

[11] Ashok, J., and Birch, J. R., "Polyethylene $(C_2H_4)n$," *Handbook of Optical Constants of Solids II*, Academic Press, New York, 1981.

[12] Spitzer, L., *Physics of Fully Ionized Gases*, Interscience, New York, 1953, Chap. 5.

[13] Zollweg, R. J., and Liebermann, R. W., "Electrical Conductivity of Nonideal Plasmas," *Journal of Applied Physics*, Vol. 62, No. 9, 1987, pp. 3621–3637. doi:10.1063/1.339265

[14] Emanuel, G., *Gasdynamics: Theory and Applications*, AIAA Education Series, AIAA, New York, 1986.

[15] Anisimov, S. I., "Vaporization of Metal Absorbing Laser Radiation," *Soviet Physics Journal of Experimental and Theoretical Physics*, Vol. 27, No. 1, 1968, pp. 182–183.

[16] Keidar, M., Boyd, I. D., and Beilis I. I, "On the Model of Teflon Ablation in a Ablation-Controlled Discharge," *Journal of Physics D: Applied Physics*, Vol. 34, No. 11, 2001, pp. 1675–1677. doi:10.1088/0022-3727/34/11/318

[17] Pekker, L., Keidar, M., and Cambier, J.-L., "Effect of Thermal Conductivity on the Knudsen Layer at Ablative Surfaces," *Journal of Applied Physics*, Vol. 103, No. 3, 2008, p. 034906. doi:10.1063/1.2838210

J. Blandino
Associate Editor